Title: Intrinsic ecological dynamics drive biodiversity turnover in model metacommunities

Authors: Jacob D. O'Sullivan[1], J. Christopher D. Terry[1], Axel G. Rossberg[1]

5th May 2020

Short title: Autonomous turnover in metacommunities

One Sentence Summary: Biodiversity change previously attributed to external drivers is explained as a robust, naturally occurring phenomenon.

Affiliations: [1]School of Biological and Chemical Sciences, Queen Mary University of London, Mile End Road, London, E1 4NS, United Kingdom

Corresponding author: Jacob Dinner O'Sullivan (j.osullivan@qmul.ac.uk), School of Biological and Chemical Sciences, Queen Mary University of London, Mile End Road, London E1 4NS, United Kingdom

Document statistics: Summary - 185 words, Main Text - 2703 words, 4 figures; Methods - 450 words; Supporting Information 2212 words, 10 figures; Citations - 67.

Keywords: biodiversity — macroecology — spatial ecology — metacommunity — community turnover — ecological structural stability

Abstract:

Turnover of species composition through time is frequently observed in nature. Often explained by changes in abiotic conditions or regional species pools, compositional turnover is employed as an indicator of external stress in natural ecosystems. Theoretically, the possibility of turnover driven by intrinsic ecological dynamics—species interactions, dispersal—is also known, but what role such *autonomous* turnover plays in nature remains unclear. Expanding the boundaries of metacommunity modelling, we show that in large metacommunities immigration pressure from neighbouring locales robustly drives continuous turnover in local composition—without environmental change or regional invasions. That ecological communities may turn over autonomously challenges assumptions implicit in assessment and management tools, and suggests that natural compositional change should be incorporated in ecological status assessments based on ancestral baselines.

Main Text:

Change in species composition through time, called community turnover, is observed in most ecosystems (*1–3*). Potential drivers include changes in the abiotic environment (*4–6*), random population fluctuations due to demographic stochasticity (*7*), and autonomous population dynamics driven by species interactions and dispersal (*8, 9*). While there exist well-developed bodies of theory describing community turnover due to environmental change (*10, 11*) and demographic stochasticity (*12*), our understanding of autonomous compositional change is underdeveloped. In particular, it remains unclear to what extent observed spatio-temporal patterns in biodiversity may be due to autonomous ecological dynamics.

If it were known that intrinsic ecological dynamics alone cannot account for observed com-

positional turnover, then abiotic environmental change would be the most plausible explanation (turnover by demographic stochasticity alone is predicted to be orders of magnitude slower than observed (*1*)). In the current phase of rapid anthropogenic environmental change, any alteration in the composition of an ecological community should then be interpreted as a potential indicator of stress (*13–15*) and the degree of compositional change compared to past baselines a valid measure of anthropogenic impact.

If, on the other hand, temporal community turnover is a natural phenomenon that can arise independently of changes in the abiotic environment, then observed shifts in the composition of ecological communities would *not* necessarily imply the presence of external pressures. Intrinsic dynamics may even permit ecosystems to adapt and absorb environmental change without impacting ecosystem functioning. Assessments, projections and mitigation strategies would then need to account for such autonomous compositional turnover.

So, can communities of many interacting species turn over autonomously? If so, what is the driving mechanism? And does the resulting turnover reproduce patterns observed in empirical data? Here we address these questions drawing on recent advances (*16*) in the theory of metacommunities (*17*), using population-dynamical simulation models with explicitly defined spatial and environmental structure. To ensure turnover is purely autonomous, we keep the environment fixed throughout simulations. In our model, local community composition is determined by *species sorting* (non-uniform responses of species to local environmental conditions and interspecific competition) and *mass effects* (immigration from neighbouring locales). The model can be understood as a simplified representation of interactions within guilds (e.g. trees or intertidal invertebrates) and has been shown to reproduce fundamental spatial biodiversity patterns (*16*).

Each of our simulated metacommunities occupies a two-dimensional landscape defined by a random spatial network, mapped onto an abiotic environment. The metacommunity is as-

sembled in a stepwise fashion by the iterative introduction of species whose numerical ecological traits are randomly sampled. There is an intrinsic limit on the number of species that can coexist in such a metacommunity (*16*). In all cases, we assemble until regional diversity reaches this asymptote; thereafter autonomous steady state dynamics are studied in the absence of regional invasions. Abiotic filtering occurs via the spatial variation of intrinsic growth rates R_{ix} and biotic filtering via interspecific competition encoded in the interaction coefficients A_{ij}. A spatial connectivity matrix with elements D_{xy} describes dispersal. Here i, j are species indices while x, y refer to patches. We model metacommunity dynamics of population biomasses $B_{ix} = B_{ix}(t)$ using a system of spatially coupled Lotka-Volterra (LV) equations that, in matrix notation, has the form (*16*)

$$\frac{d\mathbf{B}}{dt} = \mathbf{B} \circ (\mathbf{R} - \mathbf{AB}) + \mathbf{BD}, \tag{1}$$

with $\circ$ denoting element-wise multiplication.

Intrinsic growth rates R_{ix} are sampled from spatially correlated normal distributions with autocorrelation length ϕ and variance σ^2 (Fig. S1). For simplicity, and since predator-prey dynamics are known to generate fluctuations through mechanisms distinct from those we report here, we restrict our analysis to competitive communities for which all ecological interactions are antagonistic. The off-diagonal elements of the interaction matrix $\mathbf{A}$ are sampled independently from a distribution in the range $0 \leq A_{ij} < 1$ ($i \neq j$) and we set all $A_{ii} = 1$. The topology of our model metacommunities, expressed through $\mathbf{D}$, is generated by sampling the spatial coordinates of the N local communities uniformly from a $\sqrt{N} \times \sqrt{N}$ square, and linking them through a Gabriel graph (*18*). Immigration rates $D_{xy} > 0$ are then modelled using an exponential dispersal kernel with characteristic length ℓ (*19*). We selected a combination of parameters ϕ, σ^2 and ℓ that generates substantial autonomous turnover (Fig. S2) in order to obtain a full

characterisation of the phenomenon in the computationally accessible spatial range ($N \leq 256$).

Autonomous turnover in model metacommunities

For small ($N \leq 8$) metacommunities assembled to saturation in regional diversity γ, populations attain equilibria, implying the absence of autonomous turnover (*16*). With increasing metacommunity size N, however, we observe the emergence of steady-state population dynamics (Fig. S3, `https://vimeo.com/379033867`) that can produce substantial turnover in local community composition. This autonomous turnover can be represented through Bray-Curtis (*20*) (BC) similarity matrices comparing local community composition through time, and quantified by the number of compositional states detected in such matrices using hierarchical cluster analysis (*19*).

At intermediate spatial scales (Fig. 1, $16 \leq N \leq 32$) we often find oscillatory dynamics, which can be perfectly periodic or slightly irregular. With increasing oscillation amplitude, these lead to persistent turnover dynamics where local communities repeatedly fluctuate between a small number of distinct compositional states (represented in Fig. 1 by stripes of high pairwise BC similarity spanning large temporal ranges). At even larger scales ($N \geq 64$) this compositional coherence begins to break down, and for very large metacommunities ($N \geq 128$) autonomous dynamics drive continuous and unpredictable change in community composition.

Metacommunities in which the boundaries of species ranges along environmental gradients are clumped are termed *Clementsian*, while those for which range limits are independently distributed are denoted *Gleasonian* (*21*). We consider the block structure of the temporal dissimilarity matrix at intermediate N to be a form of Clementsian temporal turnover, characterized by sudden significant shifts in community composition. Metacommunity models similar to ours have been found to generate such patterns along spatial gradients (*22*), potentially via

an analogous mechanism (*23*). Large, diverse metacommunities manifest Gleasonian temporal turnover. In such cases, species invasions and extirpations are largely independent and temporal occupancies predominantly uncorrelated, such that compositional change is continuous, rarely, if ever, reverting to the same state.

Mechanistic explanation of autonomous turnover

We explain the emergence of autonomous turnover in large metacommunities building on existing analytic theory for isolated LV communities. Application of methods from statistical mechanics to models of large isolated LV communities with random interactions has revealed that such models exhibit qualitatively distinct phases (*24–26*). If the number of modelled species, S, interpreted as species pool size, lies below some threshold value determined by the distribution of interaction strengths (Fig. S4), these models exhibit a unique linearly stable equilibrium. This characterizes the so-called unique fixed point (UFP) phase. Some species may go extinct, but the majority persists (*26*). When pool size S exceeds this threshold, there appear to be no more linearly stable equilibrium configurations. Any community formed by a selection from the S species is either unfeasible (there is no equilibrium with all species present), intrinsically linearly unstable, or invadable by at least one of the excluded species. This has been called the multiple attractor (MA) phase (*25*). However, the precise nature of dynamics in this MA phase appears to remain unclear.

Ecological models have been shown to easily exhibit attractors called stable heteroclinic networks (*27*), which are characterized by dynamics in which the system bounces around between several unstable equilibria, each corresponding to a different composition of the extant community, implying indefinite community turnover. As these attractors are approached, such models exhibits increasingly long intermittent phases of slow dynamics, which, when numerically

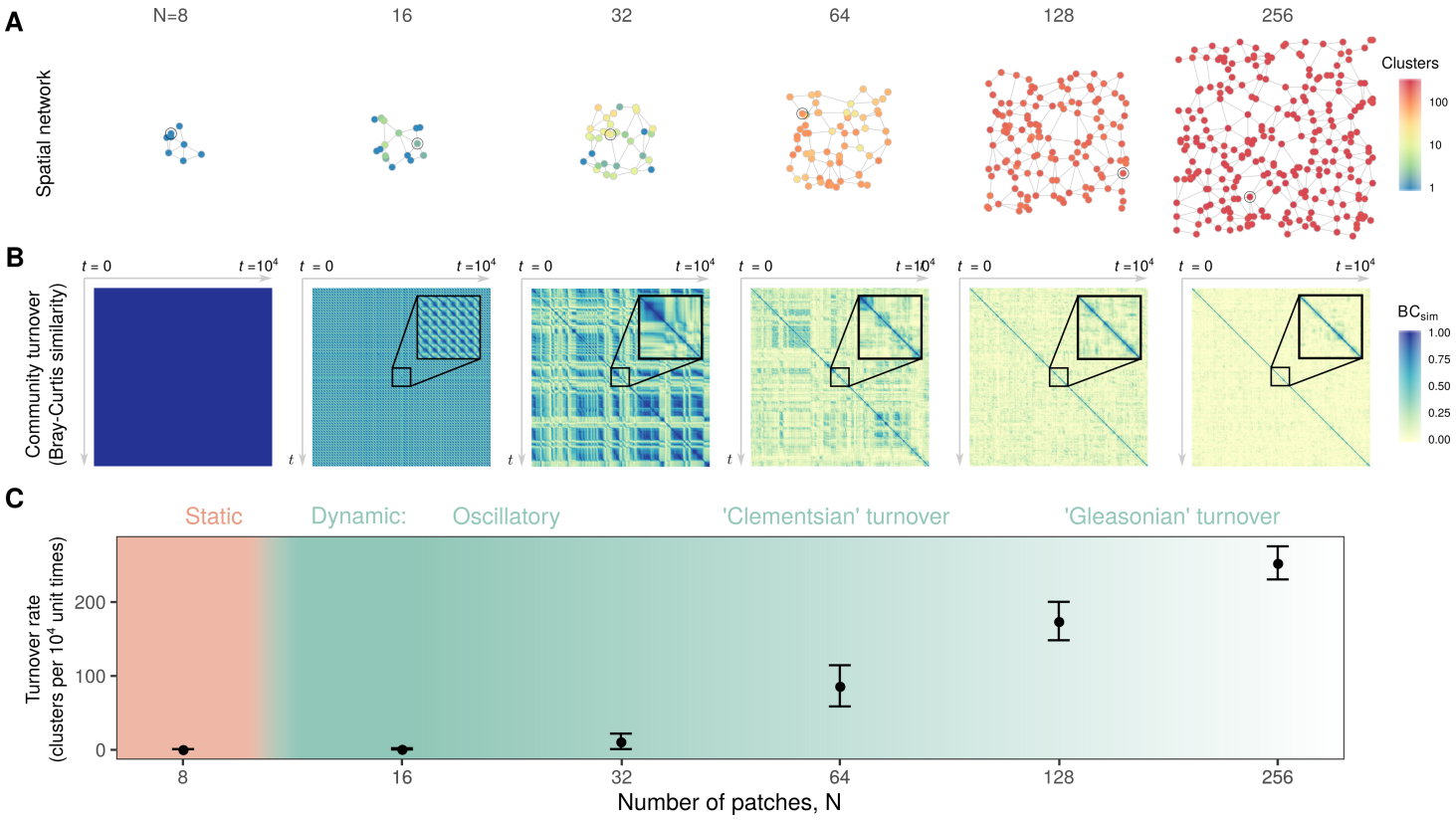

Figure 1: **Autonomous turnover in large model metacommunities.** **A**: Typical metacommunity models: a spatial network with nodes representing local communities (or patches) and edges, channels of dispersal. Node colour represents the number of local compositional states detected in 10^4 unit times using hierarchical clustering of the Bray-Curtis (BC) similarity matrix (*19*). **B**: Colour coded matrices of pairwise temporal BC similarity corresponding to the circled nodes in **A**. Insets represent 10^2 unit times. For small networks ($N = 8$) local composition converges on static fixed points. As metacommunity extent increases, however, steady state dynamics emerge. Initially this autonomous turnover is oscillatory in nature with communities fluctuating between small numbers of compositional states which can be grouped into clusters ($16 \leq N \leq 32$). Intermediate metacommunities ($32 \leq N \leq 64$) manifest 'Clementsian' temporal turnover, characterized by sharp transitions in composition, implying species turn over in cohorts. Large metacommunities ($N \geq 128$) turn over continuously, implying 'Gleasonian' assembly dynamics in which species' temporal occupancies are independent. **C**: The mean number of local compositional clusters detected for metacommunities of various numbers of patches N. While the transition from static to dynamic community composition at the local scale is sharp (see text), non-uniform turnover *within* metacommunities (**A**) blurs the transition at the regional scale. $A_{ij} = 0.5$ with probability 0.5, $\phi = 10$, $\sigma^2 = 0.01$, $\ell = 0.5$.

simulated, can give the impression that the system eventually reaches one of several 'stable' equilibria. We demonstrate in supplementary text that the MA phase is in fact characterized by stable heteroclinic networks (Figs. S5, S6). We retain the MA terminology here because the underlying complete heteroclinic networks, interpreted as a directed graph (*28, 29*), might have multiple components that are mutually unreachable through dynamic transitions (*30*), each representing a different attractor.

Spatially implicit metacommunities: To demonstrate the effect of approximate heteroclinic networks in speciose ecological models, we constructed a single-patch 'metacommuity' model: an isolated LV community coupled to an implicitly modelled local ecological neighbourhood. This is achieved by adding, for each of the S species, a propagule rain at a low rate ϵ (Eq. S5). This small perturbation, analogous to mass effects occurring in spatially explicitly metacommunity models, brings the underlying heteroclinic network in the MA phase to life (see supplementary text): because natural rates of population growth/decline are of order O(1) or smaller for this model (*31*), it prevents population biomasses from falling below levels of magnitude O(ϵ) and inhibits the indefinite slowing down of community turnover in the heteroclinic network. Here we show results for $\epsilon = 10^{-10}$ and 10^{-15}, which produce qualitatively similar outcomes: with increasing pool size S we observe a transition from stable equilibria into dynamic states in which community composition continuously turns over (*32*).

To characterize this transition quantitatively, we again performed hierarchical cluster analyses of the temporal BC similarity matrix in the model's steady state (Fig. 2A-B). For $S < 35$ (in the chosen parameterization) a single cluster was detected, generally corresponding to an equilibrium state, in rare cases superimposed with weak oscillations (Fig. 2, inset). For $S \geq 35$, autonomous compositional turnover becomes increasingly likely. Community composition can then be organised into multiple clusters, reflecting the passage of the community state past

multiple perturbed equilibria along the paths set out by the heteroclinic network of the underlying unperturbed model (Fig. 2C). As S increases, so does the complexity of the underlying attracting heteroclinic network and hence the variety of ways in which communities can form and change through time. A numerical threshold of around 35 species is consistent with the theoretical prediction (*25*) of $S \approx 32$ for the transition between the UFP and MA phases (supplementary text).

Spatially explicit metacommunities: To test whether to same mechanism drives turnover in spatially explicit metacommunity models, we defined the species pool size for a given local community as the time averaged number of species with $B_{ix} > 10^{-15}$ in the local neighbourhood, i.e. the focal patch or any adjacent patch. Under variation of metacommunity size N, we found, for systems of more than 16 local communities, a positive linear association between the number of compositional clusters detected in the time series of a focal node and the species richness of the local neighbourhood (Fig. 2D; $p < 10^{-6}$). (For $N \leq 16$ the association was non-significant because most communities were static.) Remarkably, these linear regression lines combined trace a relation between neighbourhood richness and cluster number that is very similar to that found for the single-patch model (Fig. 2D). Furthermore, the phenomenology of the gradual emergence of autonomous turnover is consistent between the single-patch model and the full metacommunity model, including the progression from oscillations, through Clementsian turnover, to Gleasonian turnover with increases in S (Fig. S7). Thus, by analogy with the single-patch LV community model, we conclude that the autonomous turnover observed in large metacommunity models is best explained by the emergence of complex, approximate heteroclinic networks at the local scale.

We have demonstrated that propagule pressure is required to perturb a local community away from unstable equilibria and drive compositional change. In order to invade, however,

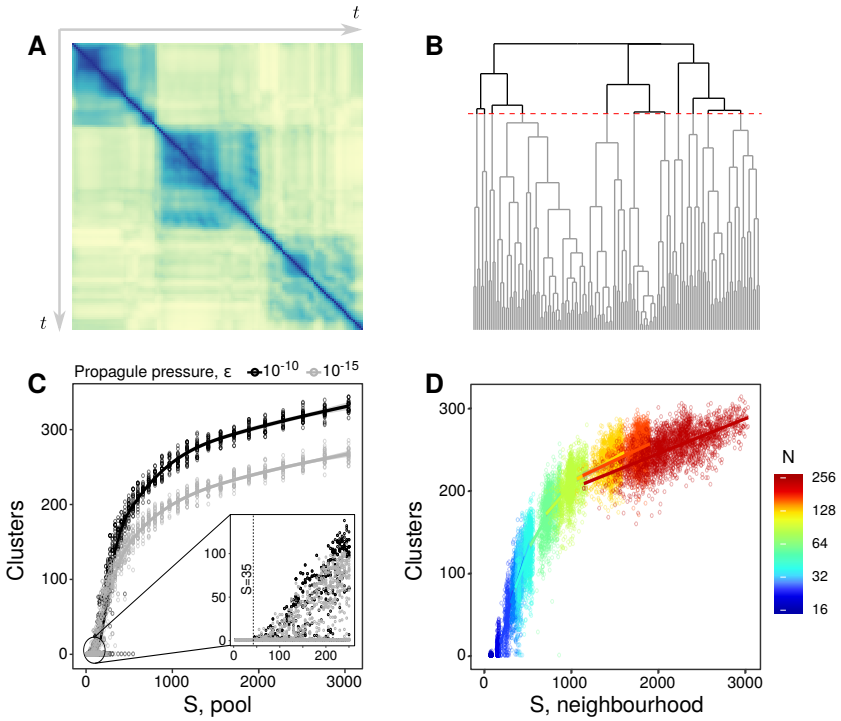

Figure 2: **Ecological mass effects drive autonomous turnover.** **A**: Compositional clustering represented by the block structure of the BC similarity matrix (200 unit times). **B**: Hierarchical cluster analysis approximately quantifies the number of compositional states with a similarity threshold of 75% (red dashed line) (*19*). **C**: The number of compositional clusters detected, plotted against the size of the pool of potential invaders for an isolated LV community using a propagule pressure ϵ of 10^{-10} and 10^{-15}, fit with a generalized additive model (*33*). For $S < 35$ a single cluster is detected. For $S \geq 35$ autonomous turnover occurs (≥ 1 compositional clusters) with the transition indicated by the dashed line (inset). **D**: Qualitatively identical behaviour was observed for model metacommunities in which 'propagule pressure' arises due to ecological mass effects from the local neighbourhood. Each point represents a single node. Lines in **D** are standard linear regressions. The good alignment of subsequent fits demonstrates that neighbourhood diversity is the dominating predictor of cluster number, rather than N. $N = 16,\ 32,\ 48,\ 64,\ 80,\ 96,\ 128,\ 160,\ 192,\ 224,\ 256$, $A_{ij} = 0.5$ with probability 0.5, $\phi = 10$, $\sigma^2 = 0.01$, $\ell = 0.5$.

species need to be capable of passing through biotic and abiotic filters. We would expect, therefore, that turnover would be suppressed in highly heterogeneous or poorly connected environments where mass effects are weak. Manipulating the parameters ϕ, σ^2 and ℓ, this is precisely what we observe (Fig. S8).

Autonomous turnover and local ecological limits: Species richness in LV systems subject to invasion pressure is ultimately regulated by the onset of ecological structural instability (*16,31*): in species rich, structurally unstable communities, press perturbations easily lead to extinctions. The boundary between the UFP and MA phases coincides exactly with the onset of structural instability (Eqs. S6-S12), implying that the emergence of biodiversity regulation and of autonomous turnover are tightly linked. For metacommunities, we demonstrate this linkage numerically in Fig. 3 by showing that, as regional species richness increases, the onset of autonomous turnover coincides with the saturation of local species richness. Autonomous turnover might therefore serve as an indication of the structural instability of complex communities.

The macroecology of autonomous turnover

We find surprising similarities between temporal and spatio-temporal biodiversity patterns emerging in model metacommunities and in empirical data (Fig. 4), with quantitative characteristics lying within the ranges observed in natural ecosystems.

Temporal occupancy: The proportion of time in which species occupy a community tends to have a bi-modal empirical distribution (*34–36*) (Fig. 4A). The distribution we found in simulations (Fig. 4E) closely matches the empirical pattern.

Community structure: Temporal turnover has been posited to play a stabilizing role in the maintenance of community structure (*37,38*). In an estuarine fish community (*39*), for example,

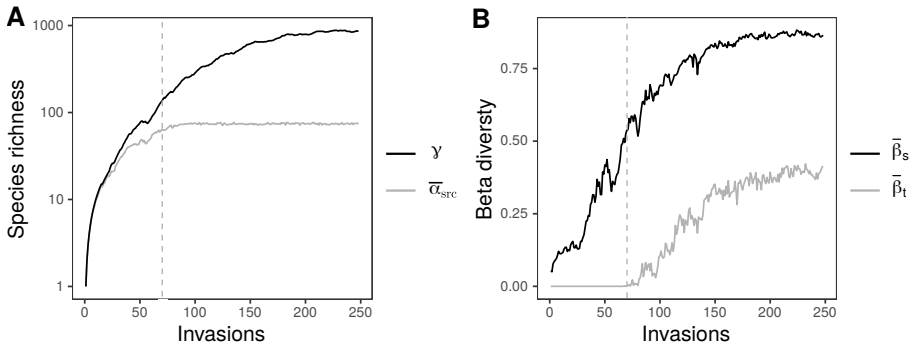

Figure 3: **The emergence of temporal turnover during metacommunity assembly**. **A**: Species richness at local ($\overline{\alpha}_{\text{src}}$, grey) and regional scales (γ, black) for a single metacommunity of $N = 32$ coupled communities during iterative invasion of random species. We quantify local source diversity $\overline{\alpha}_{\text{src}}$ as the metacommunity average of the number α_{src} of non-zero equilibrium populations persisting when immigration is switched off (off-diagonal elements of $\mathbf{D}$ set to zero), since this is the component of a local community subject to strict ecological limits to biodiversity. Note the log scale chosen for easy comparison of local and regional richness. **B**: Increases in regional diversity beyond local limits arise via corresponding increases in spatial turnover ($\overline{\beta}_{\text{s}}$, black). Autonomous temporal turnover ($\overline{\beta}_{\text{t}}$, grey) sets in precisely when average local species richness $\overline{\alpha}_{\text{src}}$ has reached its limit, reflecting the equivalence of the transition to the MA phase space and the onset of local structural instability. In both panels, the dashed line marks the point at which autonomous temporal turnover was first detected. $A_{ij} = 0.3$ with probability 0.3, $\phi = 10$, $\sigma^2 = 0.01$, $\ell = 0.5$.

species richness (Fig. 4B) and the distribution of abundances were remarkably robust despite changes in population biomasses by multiple orders of magnitude. In model metacommunities with autonomous turnover we found, likewise, that local species richness exhibited only small fluctuations around the steady-state mean (Fig. 4F, three random local communities shown) and that the macroscopic structure of the community was largely time invariant (Fig. S9). In the light of our results, we propose the absence of temporal change in community properties such as richness or abundance distribution despite potentially large fluctuations in population abundances (*39*) as an indication of predominantly autonomous ecological dynamics.

The Species-Time-Area-Relation, STAR: The species-time-relation (STR), typically fit by a power law of the form $S \propto T^w$, describes how observed species richness increases with observation time T. The exponent w of the STR has been found to be remarkably consistent across taxonomic groups and ecosystems (*40–42*), indicative of some general population dynamical mechanism. However, the exponent of the STR decreases with increasing sampling area (*40*), and the exponent of the empirical Species Area Relation (SAR) ($S \propto A^z$) consistently decreases with increasing sampling duration (*40*) (Fig. 4C, D). We tested for this pattern in a large simulated metacommunity with $N = 256$ patches by computing the STAR for nested subdomains and variable temporal sampling windows (*19*). We observed exponents of the nested SAR in the range $z = 0.25$-0.60 and for the STR a range $w = 0.02$-0.48 (Fig. S10), both in good agreement with observed values (*41, 43*). We also found a clear decrease in the rate of species accumulation in time as a function of sample area and vice-versa (Fig. 4G, H).

Thus, the distribution of temporal occupancy, the time invariance of key marcoecological structures and the STAR in model metacommunities match observed patterns. This evidence suggests that such autonomous dynamics cannot be ruled out as an important driver of temporal compositional change in natural ecosystems.

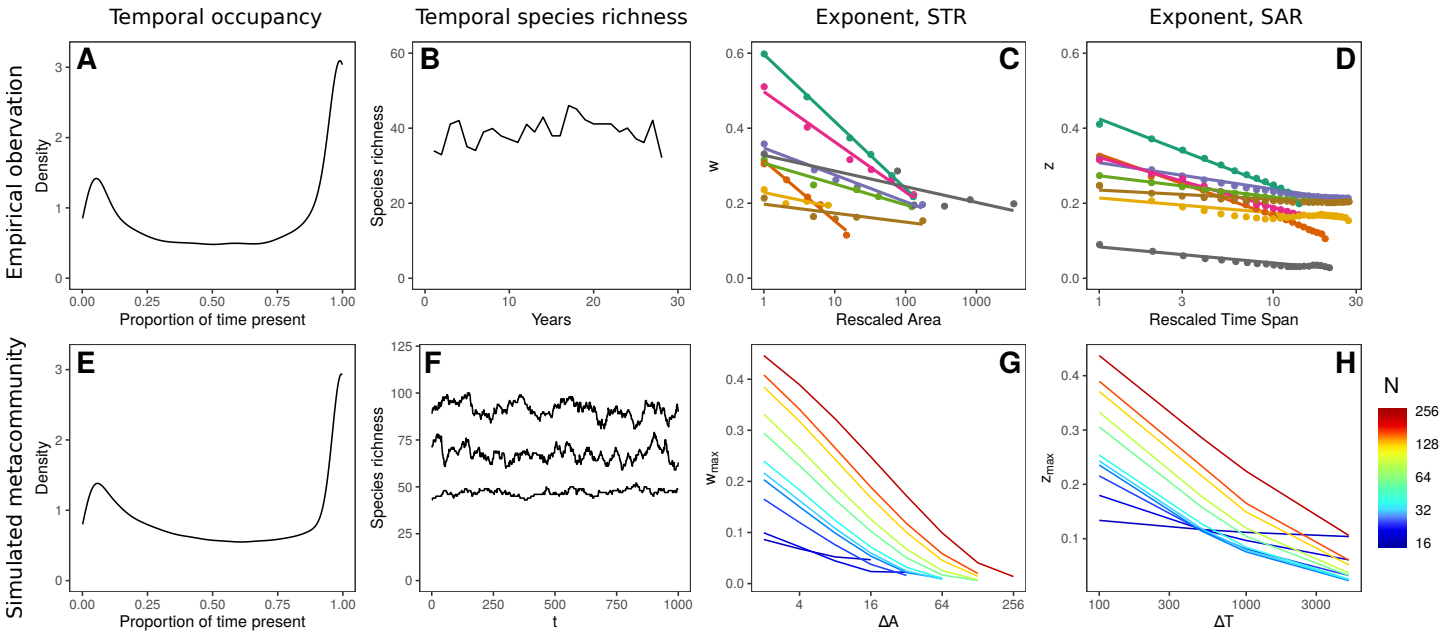

Figure 4: **Macroecological signatures of autonomous compositional change**. A bimodal distribution in temporal occupancy observed in North American birds (*34*) (**A**) and in simulations (**E**, $N = 64$, $\phi = 5$, $\sigma^2 = 0.01$, $\ell = 0.5$). Intrisically regulated local species richness observed in estuarine fish species (*39*) (**B**) and in simulations (**F**, $N = 64$, $\phi = 5$, $\sigma^2 = 0.01$, $\ell = 0.5$). The decreasing slopes of the STR with increasing sample area (*40*) (**C**), and the SAR with increasing sample duration (*40*) (**D**) for various communities and in simulations (**G** and **H**, $N = 256$, $\phi = 10$, $\sigma^2 = 0.01$, $\ell = 0.5$). In **C** and **D** we have rescaled the sample area/duration by the smallest/shortest reported value and coloured by community (see original study for details). In **G** and **H** we study the STAR in metacommunities of various size N, represented by colour. Limited spatio-temporal turnover in the smallest metacommunties (blue colours) greatly reduces the exponents of the STAR relative to large metacommunities (red colours). $A_{ij} = 0.5$ with probability 0.5 in all cases.

Conclusions

Current understanding of the mechanisms driving temporal turnover in ecological communities is predominantly built upon phenomenological studies of observed patterns (*44*) and is unquestionably incomplete (*39, 45*). That temporal turnover can be driven by external forces – seasonal or long term climate change, direct anthropogenic pressures etc. – is indisputable. A vitally important question is, however, how much empirically observed compositional change is actually due to such forcing. A recent landmark analysis of temporal patterns in biodiversity detected no systematic change in species richness or structure in natural communities, despite rates of compositional turnover greater than predicted by null models (*1–3, 46*). Here we have shown that empirically realistic turnover in model metacommunities can occur via precisely the same mechanism as that responsible for regulating species richness at the local scale. While the processes regulating diversity in natural communities remain poorly understood, our theoretical work suggests local structural instability may explain these empirical observations in a unified and parsimonious way.

Simulations reveal a qualitative transition from small to large metacommunities. For communities of species such as marine mammals or large fish whose ranges can extend across entire macroclimatic niches, one might plausibly expect that autonomous turnover is absent. For organisms with ranges that are small compared to their macroclimatic niches, on the other hand, autonomous turnover of local communities can plausibly be expected based on our findings. Empirically distinguishing between these two cases for different guilds will be an important task for the future.

At intermediate spatial scales, autonomous turnover is characterized by sharp transitions between cohesive compositional states. To date, few empirical analyses have reported such coherence in temporal turnover, perhaps because the taxonomic and temporal resolution required

to detect such patterns is not yet widely available. Developments in biomonitoring technologies (*47*) are likely to reveal a variety of previously undetected ecological dynamics, however. By combining high resolution temporal sampling and metagenetic analysis of community composition, a recent study demonstrated cohesive but short-lived community cohorts in coastal plankton (*48*). Such Clementsian temporal turnover may offer a useful signal of autonomous compositional change in real systems.

Thus, overcoming previous computational limits to the study of complex metacommunities (*49, 50*), we have discovered the existence of two distinct phases of metacommunity ecology—one characterized by weak or absent autonomous turnover, the other by continuous compositional change in the absence of external drivers. By synthesizing a wide range of established ecological theory (*16, 25, 27, 49*), we were able to heuristically explain these phases. Our explanation implies that autonomous turnover requires little more than a diverse neighbourhood of potential invaders, a weak immigration pressure, and a complex network of interactions between co-existing species.

Acknowledgements: We thank Lars Chittka and Laurent Frantz for comments on earlier drafts of this paper. **Funding:** This work forms part of the project "Mechanisms and prediction of large-scale ecological responses to environmental change" funded by the Natural Environment Research Council (NE/T003510/1). **Author contributions:** AGR conceived of the study. JDO and AGR designed the model. JDO developed the model, performed simulations, analysed the data and drafted the manuscript. All authors interpreted model outputs in comparison with observations and contributed to manuscript writing. **Competing interests:** The authors declare no competing interests. **Data and materials availability:** Should this manuscript be accepted simulation data supporting the results will be archived in a public repository and the data DOI will be included at the end of the article.

References and Notes

1. M. Dornelas, *et al.*, *Science* **344**, 296 (2014).

2. N. J. Gotelli, *et al.*, *Science Advances* **3**, e1700315 (2017).

3. M. Vellend, *et al.*, *Proceedings of the National Academy of Sciences of the United States of America* **110**, 19456 (2013).

4. R. J. Hobbs, S. Yates, H. A. Mooney, *Ecological Monographs* **77**, 545 (2007). WOS:000250915400004.

5. C. Kampichler, C. A. M. van Turnhout, V. Devictor, H. P. van der Jeugd, *PloS One* **7**, e35272 (2012).

6. T. Newbold, *et al.*, *Nature* **520**, 45 (2015).

7. N. G. Swenson, *et al.*, *Ecology* **93**, 490 (2012).

8. J. H. Connell, R. O. Slatyer, *The American Naturalist* **111**, 1119 (1977).

9. B. L. Brown, R. L. Lawson, *Ecology* **91**, 1799 (2010).

10. J. Elith, J. R. Leathwick, *Annual Review of Ecology, Evolution, and Systematics* **40**, 677 (2009).

11. M. Kearney, W. Porter, *Ecology Letters* **12**, 334 (2009).

12. S. P. Hubbell, *The Unified Neutral Theory of Biodiversity and Biogeography (MPB-32)* (Princeton University Press, 2001).

13. European Commission, Common Implementation Strategy for the Water Framework Directive (2000/60/EC), Guidance Document no. 5, Official journal of the European communities (2003).

14. European Commission, Common Implementation Strategy for theWater Framework Directive (2000/60/EC), Guidance Document no. 10, Official journal of the European communities (2003).

15. A. E. Magurran, *et al.*, *Proceedings of the National Academy of Sciences* **115**, 1843 (2018).

16. J. D. O'Sullivan, R. J. Knell, A. G. Rossberg, *Ecology Letters* **22**, 1428 (2019).

17. M. A. Leibold, *et al.*, *Ecology Letters* **7**, 601 (2004).

18. K. R. Gabriel, R. R. Sokal, *Systematic Zoology* **18**, 259 (1969).

19. Detailed Materials and Methods are available as Supplementary Materials.

20. J. R. Bray, J. T. Curtis, *Ecological Monographs* **27**, 325 (1957).

21. M. A. Leibold, G. M. Mikkelson, *Oikos* **97**, 237 (2002).

22. K. Liautaud, E. H. van Nes, M. Barbier, M. Scheffer, M. Loreau, *Ecology Letters* **22**, 1243 (2019).

23. J.-F. Arnoldi, M. Barbier, R. Kelly, G. Barabás, A. L. Jackson, *Preprint at https://www.biorxiv.org/content/10.1101/705756v2* p. 705756 (2019).

24. H. Rieger, *Journal of Physics A: Mathematical and General* **22**, 3447 (1989).

25. G. Bunin, *Physical Review E* **95**, 042414 (2017).

26. T. Galla, *EPL (Europhysics Letters)* **123**, 48004 (2018).

27. J. Hofbauer, *Equadiff 8* pp. 105–116 (1994).

28. R. Law, R. D. Morton, *Ecology* **74**, 1347 (1993).

29. D. A. Kessler, N. M. Shnerb, *Physical Review E* **91**, 042705 (2015).

30. S. N. Dorogovtsev, J. F. F. Mendes, A. N. Samukhin, *Physical Review E* **64**, 025101 (2001).

31. A. G. Rossberg, *Food Webs and Biodiversity: Foundations, Models, Data* (John Wiley & Sons, 2013).

32. F. Roy, M. Barbier, G. Biroli, G. Bunin, *Preprint at https://www.biorxiv.org/content/10.1101/730820v1* (2019).

33. T. J. Hastie, R. J. Tibshirani, *Monographs on statistics and applied probability* p. 15 (1990).

34. J. R. Coyle, A. H. Hurlbert, E. P. White, *The American Naturalist* **181**, E83 (2013).

35. M. F. Jenkins, E. P. White, A. H. Hurlbert, *PeerJ* **6** (2018).

36. S. J. S. Taylor, B. S. Evans, E. P. White, A. H. Hurlbert, *Ecology* **99**, 1825 (2018).

37. D. F. Doak, *et al.*, *The American Naturalist* **151**, 264 (1998).

38. D. Tilman, C. L. Lehman, C. E. Bristow, *The American Naturalist* **151**, 277 (1998).

39. A. E. Magurran, P. A. Henderson, *Philosophical Transactions of the Royal Society B: Biological Sciences* **365**, 3611 (2010).

40. P. B. Adler, *et al.*, *Ecology* **86**, 2032 (2005).

41. E. P. White, *et al.*, *Oikos* **112**, 185 (2006).

42. A. Shade, J. G. Caporaso, J. Handelsman, R. Knight, N. Fierer, *The ISME Journal* **7**, 1493 (2013).

43. S. Drakare, J. J. Lennon, H. Hillebrand, *Ecology Letters* **9**, 215 (2006).

44. E. P. White, M. A. Gilchrist, *Evolutionary Ecology Research* **9**, 1329 (2007).

45. A. E. Magurran, M. Dornelas, F. Moyes, P. A. Henderson, *Global Ecology and Biogeography* **28**, 1949 (2019).

46. F. A. M. Jones, A. E. Magurran, *Biology Letters* **14**, 20180187 (2018).

47. D. A. Bohan, *et al.*, *Trends in Ecology & Evolution* **32**, 477 (2017).

48. A. M. Martin-Platero, *et al.*, *Nature Communications* **9**, 1 (2018).

49. R. Law, M. A. Leibold, *Metacommunities: Spatial Dynamics and Ecological Communities*, M. Holyoak, M. A. Leibold, R. D. Holt, eds. (University of Chicago Press, 2005).

50. M. Hamm, B. Drossel, *Preprint at https://www.biorxiv.org/content/10.1101/810390v1* (2019).

Supplementary references

51. R. J. Adler, *The Geometry of Random Fields* (SIAM, 2010).

52. R. A. Johnson, D. W. Wichern, *Applied Multivariate Statistical Analysis*, vol. 5 (Prentice hall Upper Saddle River, NJ, 2002).

53. T. King, S. Butcher, L. Zalewski (2017).

54. J. Oksanen, *et al.*, *Community ecology package, version* **2** (2013).

335 55. P. Legendre, L. Legendre, *Numerical Ecology* (Elsevier, 2012), third edn.

336 56. A. Baselga, *Methods in Ecology and Evolution* **8**, 799 (2017).

337 57. A. Baselga, C. D. L. Orme, *Methods in Ecology and Evolution* **3**, 808 (2012).

338 58. J. B. Shurin, *et al.*, *Ecology Letters* **10**, 127 (2007).

339 59. R. Ptacnik, *et al.*, *Proceedings of the National Academy of Sciences* **105**, 5134 (2008).

340 60. R. Ptacnik, T. Andersen, P. Brettum, L. Lepistö, E. Willén, *Proceedings of the Royal Society*
341 *B: Biological Sciences* **277**, 3755 (2010).

342 61. J. J. Korhonen, J. Soininen, H. Hillebrand, *Ecology* **91**, 508 (2010).

343 62. J. C. Stegen, *et al.*, *Global Ecology and Biogeography* **22**, 202 (2013).

Supplementary materials

Materials and Methods

Supplementary text

Figs. S1 – S10

Materials and Methods

Metacommunity assembly: The dynamics of local population biomasses $B_{ix}(t)$ were modelled using a spatial extension to the multispecies Lotka-Volterra competition model (*16*):

$$\frac{dB_{ix}}{dt} = B_{ix}\left(R_{ix} - \sum_{j=1}^{S} A_{ij}\, B_{jx}\right) - e\, B_{ix} + \sum_{y \in \mathcal{N}(x)} \frac{e}{k_y} \exp\left(-d_{xy}\ell^{-1}\right) B_{iy}. \qquad \text{(S1)}$$

The competitive coupling coefficients A_{ij} for $i \neq j$ were sampled from discrete distributions. Generally, A_{ij} were set to 0.5 with a probability of 0.5 and to 0 otherwise, however, for the simulation shown in Fig. 3, we relaxed the dynamic coupling and instead set A_{ij} to 0.3 with a probability of 0.3. This delayed the onset of local structural instability during metacommunity assembly, making the coincident emergence of local diversity regulation and autonomous compositional turnover visually clearer.

Environmental heterogeneity was modelled implicitly through spatial variation in species' intrinsic growth rates R_{ix}. Specifically, the R_{ix} were sampled independently for each species i from a Gaussian random field (*51*) with mean $\mu = 1.0$ and standard deviation σ, generated via spectral decomposition (*52*) of the $N \times N$ landscape covariance matrix with elements $\Sigma_{xy} = \exp\left[-\phi^{-1} d_{xy}\right]$, where d_{xy} denotes the Euclidean distances between patches x and y, and ϕ the autocorrelation length (Fig. S1).

The dispersal matrix $\mathbf{D}$ (Eq. (1)) has diagonal elements D_{xx} of $-e$, where e, the fraction of biomass leaving patch x per unit time, was kept fixed at 0.01 for all simulations. For pairs

of nodes connected by an edge in the spatial network, the immigration terms were modelled as negative exponentials $D_{xy} = ek_y^{-1} \exp\left(-d_{xy}\ell^{-1}\right)$, controlled by a dispersal length parameter ℓ, thus assuming a propensity for propagules to transition to nearby sites. The normalisation constant k_y divides the biomass departing patches y between all other patches in *its* local neighbourhood ($\mathcal{N}(y)$), weighted by the ease of reaching each patch i.e. $k_y = \sum_{z\in\mathcal{N}(y)} \exp\left(-d_{yz}\ell^{-1}\right)$, implying an active dispersal process.

Metacommunities were assembled through a stepwise invasion process. In each iteration of the algorithm, $0.05S + 1$ new species were introduced to the the metacommunity, with S denoting the current extant species richness. The invaders were tested to ensure positive growth rates at low abundance, and then added at 10^{-6} biomass units to the local community in which their growth rate was highest. The metacommunity was periodically scanned and species with biomass smaller than 10^{-4} biomass units in all nodes of the network were considered regionally extinct and removed from the model. The assembly algorithm aims to remove all species whose total biomass declines to zero in the course of the system's complex dynamics. In rare cases autonomous fluctuations may drive one of the remaining species to very low abundance in all nodes, however the majority retain local biomass above the detection threshold in at least one node at all times.

To assemble models of sufficient spatial extent and species richness, we developed a parallel implementation of the assembly algorithm based on a domain decomposition of the spatial network, and simulated it on the high-performance cluster at Queen Mary, University of London (*53*). This permitted assembly of saturated metacommunities of up to $N = 256$ patches harbouring $S \sim 3000$ species, thus breaking through frequently lamented computational limits (*49, 50*) on the numerical study of metacommunities.

Quantifying autonomous turnover: For fully assembled metacommunities, we simulated and stored time series of $t_{\max} = 10^4$ metacommunity samples $B_{ixt} = B_{ix}(t)$ taken in intervals of one unit time. In these metacommunity timeseries, we measured spatio-temporal turnover based on i) compositional dissimilarity, ii) the distribution of temporal occupancy, iii) the number of compositional clusters detected using hierarchical clustering, and iv) via species accumulation curves generated using sliding spatial and temporal sampling windows. Metrics were selected in order to answer specific questions, or for comparison to observed patterns. Some analyses require quantifying local species richness. This was done by setting a detection threshold of 10^{-4} biomass units, below which populations are considered absent from the community. *Local source diversity*, which we define in Fig. 3, is a related but different diversity measure that is more adequate for quantifying the component of a local community subject to local ecological limits to biodiversity.

Compositional dissimilarity: Spatio-temporal compositional similarity was quantified using the Bray-Curtis (*20*) similarity index via the function `vegdist` in the R package "vegan" (*54*).

Temporal occupancy: We assessed temporal occupancy by first converting biomass into presence-absence data ($P_{ixt} = 1$ for all $B_{ixt} > 10^{-4}$, and 0 otherwise). Then, for all populations present at least once, we computed the temporal occupancy (TO_{ix}) as the proportion of the time interval of length $t_{\max}$ during which that population was present:

$$TO_{ix} = \frac{1}{t_{\max}} \sum_t P_{ixt} \tag{S2}$$

Hierarchical clustering: We assessed the degree of temporal clustering in community composition using complete linkage hierarchical clustering (*55*) of the Bray-Curtis similarity matrix, which gives an approximate measure of the number of unstable equilibria between which the

dynamical system fluctuates. We computed the number of clusters using a threshold of 75% similarity, which reflects the structure visible in pairwise dissimilarity matrices (Fig. 2A and B).

Spatio-temporal species accumulation: We studied the STR and SAR in model metacommunities using a sliding window approach, asking how many species S^{obs} were detected in spatial 'windows', represented by connected sub-graphs of ΔA nodes, during temporal windows of ΔT unit times:

$$S^{\text{obs}} = \sum_{i} \left[\sum_{t \in \Delta T} \sum_{x \in \Delta A} P_{ixt} \geq 1 \right] \tag{S3}$$

where the Iverson brackets $[.]$ denote the indicator function. Time windows with all possible starting points for a given window length were evaluated and analogously for the spatial subsampling, and then the average species richness for a given sample size computed. In closed systems, the species accumulation in both space and time must ultimately saturate, either when the entire metacommunity or entire time series is sampled. Thus we defined the exponents z and w of the STAR as the maximum slopes of the SAR/STR on double logarithmic axes (Fig. S10).

Supplementary text

Spatial parameterization: Other than patch number N, the parameters that most impact the spatio-temporal structure of model metacommunities are the environmental correlation length ϕ, the variability of the environment σ^2, and the dispersal length ℓ. In order to understand the role of these parameters for autonomous turnover, we fixed $N = 64$ and assembled metacommunity models with σ^2, $\ell = 1 \times 10^{-2}$, 5×10^{-2}, 1×10^{-1}, 5×10^{-1}, 1, and $\phi = 1,\ 5,\ 10,\ 50,\ 100$ in all combinations and computed the resulting temporal beta diversity as the mean spatially averaged temporal BC dissimilarity observed in 10 replicates

of each parameterization. Rates of autonomous turnover varied in a complex but systematic way under variation in the spatial parameterization of the model, with turnover being weakly correlated with the dispersal length and maximized for intermediate habitat heterogeneity and autocorrelation (Fig. S2). Weak abiotic heterogeneity seeds the non-uniform spatial structure of the metacommunity and therefore promotes turnover. For large enough spatial networks, dispersal limitation and competitive repulsion alone are sufficient to drive steady state dynamics in perfectly uniform landscapes. The scan of the parameter space allowed selection the parameterization that maximized autonomous turnover: $\phi = 10$, $\sigma^2 = 0.01$, $\ell = 0.5$ (peak in Fig. S2A). Using this combination of parameters we then assembled metacommunity models of $N = 8,\ 16,\ 32,\ 48,\ 64, 80,\ 96,\ 128,\ 160,\ 192,\ 224,\ 256$. By maximizing turnover in this way, we were able to explore the macroecological implications of autonomous turnover in the computationally accessible spatial range ($N \leq 256$).

To some extent, the complex roles of parameters ϕ, σ^2, and ℓ, shown in Fig. S2, can be distilled into the effect on a single parameter: the time averaged spatial community dissimilarity at the local neighbourhood scale. To demonstrate this we used the multiple-site dissimilarity metric derived in Ref. (*56*), which generates an unbiased total beta diversity metric for systems of three or more sites/time points, allowing direct comparison of beta diversity for local neighbourhoods of different numbers of nodes. Spatial β-diversity, β_s, was computed using the function `beta.multi.abund()` included in the R package 'betapart' (*57*). This metric partitions β-diversity into two components corresponding to species replacement and compositional nestedness. Here we report total dissimilarity only. Temporal turnover responded unimodally to local neighbourhood dissimilarity (Fig. S8) over the parameter range of Fig. S2, suggesting that spatial parameterizations that maximise β_s, either through exaggerating abiotic differences between adjacent local communities or dampening mass effects, can *elevate* neighbourhood diversity while simultaneously *suppressing* the pool of species that can actually

invade.

This result makes plausible why empirical studies have detected a range of statistical associations between spatial and temporal turnover in natural ecosystems. Positive, negative, unimodal, and non-significant relationships have been reported between temporal turnover and species richness or spatial turnover (*41*), (*58–62*). The unimodal response, shown in Fig. S8 may help to resolve these apparent contradictions: it is not species richness or spatial dissimilarity *per se* that best predict temporal turnover, but the size of the pool of species capable of passing through biotic and abiotic filters to invade a local community.

Note that for consistency we compute β_t in Fig. S8 using the BC dissimilarity as in Fig. S2, however the pattern is qualitatively unchanged if β_t is computed using alternative β-diversity metrics or cluster analysis as in the main text.

Phase space of a generalised Lotka-Volterra community: Analytic theory (*25*) predicts a sharp transition between what has been called the Unique Fixed Point (UFP) and Multiple Attractor (MA) phases. In Fig. S4 we reproduce the phase portrait for such a system and note that our explicitly modelled metacommunities reveal a gradual transition in the MA phase space from oscillatory, to Clementsian and into Gleasonian turnover regimes. Assuming large S, the sharp transition between UFP and MA phases has been shown (*25*) to occur at species richness

$$S = \frac{2}{(1+\gamma)^2 \operatorname{var}(A_{ij})}, \tag{S4}$$

where $\gamma = \operatorname{corr}(A_{ij}, A_{ji})$ denotes the degree of correlation in the effects two species have on each other, measuring the symmetry of interspecific interaction strengths, and $\operatorname{var}(A_{ij})$ is the variance in the distribution. In our model we use a random interaction matrix for which $\gamma = 0$. We sample interaction coefficients from a discrete distribution with $\operatorname{var}(A_{ij}) = (0.25)^2$ giving

a predicted transition into the MA phase space at $S = 32$ species. Thus, while the prediction is approximate for small S communities with non-uniform intrinsic growth rates, a numerically observed threshold of around 35 species in the isolated LV model (Fig. 2C inset) is consistent with these analytic predictions.

Isolated LV communities: To explore the emergence of heteroclinic networks in LV models, we studied an isolated LV model with and without coupling to an implicitly modelled neighbourhood species pool. The dynamics of the model follow

$$\frac{d\mathbf{b}}{dt} = \mathbf{b} \circ (\mathbf{r} - \mathbf{A}\mathbf{b}) + \boldsymbol{\epsilon}, \tag{S5}$$

where $\mathbf{b}$ is a population biomass vector of length S, $\mathbf{r}$ is a vector of independent random normal variables with mean 1 and variance $\sigma^2 = 0.01$ representing maximum intrinsic growth rates, $\mathbf{A}$ is a competitive overlap matrix and the vector $\boldsymbol{\epsilon}$ represents the slow immigration of biomass corresponding to a weak propagule pressure. The elements ϵ_i are analogous the to explicitly modelled immigration terms $B_{ix}D_{xy}$ of the full metacommunity model.

As in the metacommunity model, interspecific competition coefficients A_{ij} were set to 0.5 with a probability of 0.5 for $i \neq j$ and otherwise to zero, while $A_{ii} = 1$, for all i. We enforced $b_i > 0$ for all i by simulating dynamics in terms of logarithmic biomass variables. In simulating this model, we did not follow the common practice of removing species whose biomass drops below some threshold. Instead all species were retained. We consider two situations: with and without the inclusion of a weak propagule pressure $\boldsymbol{\epsilon}$.

Heteroclinic networks in the case without propagule pressure: We first demonstrate in simulations that, indeed, as predicted under certain constraints (*27*), stable heteroclinic networks exist in the MA phase of model Eq. (S4) for $\boldsymbol{\epsilon} = 0$. For this we choose $S = 300$,

which, with other parameters set as described above, brings us deeply into the MA phase of the model. Simulations were initialised by setting all $B_i = 10^{-3}$ ($1 \leq i \leq S$) at $t = 0$. The system was simulated until $t = 2.1 \cdot 10^7$ and system states recorded at times $t = 2.1 \cdot 10^{j/1000}$ ($0 \leq j \leq 7000$). As illustrated in Fig. S5, while dynamics tend to become slower for larger t, no stable equilibrium or other simple attractor appears to be ever reached—as expected for a system approaching a heteroclinic network. Instead, as expected when a heteroclinic network exists, the system bounces around between unstable equilibria, apparently in a random fashion. Unexpected to us, however, the system appears to visit not only unstable equilibria in its transient, but occasionally also unstable periodic orbits ($t \approx 1.3 \cdot 10^4$ in Fig. S5) and perhaps more complex invariant sets ($t \approx 1.2 \cdot 10^6$ in Fig. S5).

One might wonder whether there is any tendency for dynamics to eventually come to a halt. To study this question, we calculated the number of changes in community composition (species invasions and extinctions) between all pairs of subsequently recorded system states, where we considered a species i as "present" if $B_i > 10^{-4}$, and from this the momentary rate of change in composition on the $\ln(t)$ scale by dividing by $\ln(10^{1/1000})$. In Fig. S6 we show the time series of the centred moving average over this number for 100 subsequent pairs or recordings, and averages for non-overlapping adjacent blocks for 300 pairs. Spikes where the rate of change is particularly high correspond to brief phases of regular or irregular oscillation. We performed a median regression of the block-wise averages by a power law (rate) $\sim t^\nu$. Median regression was used to de-emphasize the spikes. For the simulation shown in Fig. S5 found that ν did not differ significantly from zero, implying a decline of the turnover rate on the natural time axis as t^{-1}. When we repeated this analysis for 15 independent simulations (two of which failed due to numerical issues), we observed a tendency for ν to be slightly positive ($\nu = 0.054 \pm 0.020$, t-test $t = 2.67$, $p = 0.020$), perhaps because the effect of oscillatory phases on the mean turnover rate on the $\ln(t)$-scale increases with increasing t. Overall, however, the decline of turnover

rate approximately as t^{-1} was confirmed, providing evidence for the existence of an attracting heteroclinic network that the LV system Eq. (S5) with $\boldsymbol{\epsilon} = 0$ slowly approaches.

Use of logarithmic biomass variables was essential for these simulations. We found that median species biomass at the end of each run was typically around $10^{-3,500,000}$, much smaller than the smallest number representable by double precision floating point arithmetic, which is around $2 \cdot 10^{-308}$. Needless to say, these small numbers mean that the simulations with $\epsilon = 0$ are, while instructive, ecologically unrealistic.

Heteroclinic networks in the case with propagule pressure: The case $\boldsymbol{\epsilon} > 0$, where dynamics move alongside the underlying heteroclinic network without ever fully approaching it, is discussed in the Main Text as it provides a useful intermediate between the explicit metacommunity model and the more tractable isolated community. In Fig. S7 we show that the transition from oscillatory to Clementsian and finally Gleasonian turnover regimes can also be observed in these isolated LV models ($\epsilon_i = \epsilon = 10^{-15}$ for all i, other parameters as above).

Local structural instability drives autonomous turnover: Species richness in competitive LV communities is intrinsically limited by the onset of ecological structural instability. Here we show analytically that for isolated communities the boundary between the UFP and MA phases (*25*) is identical to the structurally unstable limit (*31*).

The transition between UFP and MA phase for competitive LV models occurs (*25*) when

$$\Phi = (u - \gamma v)^2 , \tag{S6}$$

where $\Phi \coloneqq S^*/S$ is the proportion of species persisting, i.e. the ratio between the number S^* of species that persist and the pool size S, and again $\gamma = \mathrm{cor}\,(A_{ij}, A_{ji})$. The quantities u and v in Eq. (S6) are given by

$$u = \frac{1 - \mathsf{E}[A_{ij}]}{S^{1/2}\,\mathrm{std}\,(A_{ij})}, \tag{S7}$$

with $\mathsf{E}[A_{ij}]$ and $\mathrm{std}\,(A_{ij})$ denoting mean and standard deviation of the distribution of off-diagonal entries of $\mathbf{A}$, respectively, and

$$v = \frac{\Phi}{u - \gamma v}. \tag{S8}$$

For $\gamma \neq 0$, Eq. (S8) does not have a unique solution for v. The equivalent quadratic equation $\gamma v^2 - uv + \Phi = 0$ has two solutions, one of which diverges as $\gamma \to 0$; this we discard. The other solution is

$$v = \frac{u - \sqrt{u^2 - 4\gamma\Phi}}{2\gamma}, \tag{S9}$$

which becomes $v = \Phi/u$ for $\gamma \to 0$, consistent with Eq. (S8). Substitution of Eq. (S9) into Eq. (S6) gives

$$\Phi = \left(\frac{u - \sqrt{u^2 - 4\gamma\Phi}}{2}\right)^2, \tag{S10}$$

which can be shown in a standard calculation to be equivalent to

$$\Phi = \frac{u^2}{(1+\gamma)^2} \tag{S11}$$

for $u > 0$ and $-1 < \gamma < 1$. Finally, substituting Eq. (S7) into Eq. (S11) gives

$$S^* = \frac{\left(1 - \mathsf{E}[A_{ij}]\right)^2}{(1+\gamma)^2 \operatorname{var}(A_{ij})}, \tag{S12}$$

which is exactly the theoretical limit of structural instability in isolated LV communities [Eq. (18.3) of Ref. 31], thus demonstrating that UFP-MA phase boundary and the onset of structural instability perfectly coincide.

Temporal patterns in community structure: Fluctuations in local population biomasses as communities move between unstable equilibria in heteroclinic networks can span multiple orders of magnitude (red trajectories in Fig. S9A) and lead to significant temporal turnover in community composition (Fig. S9B). In contrast, the high-level properties of the assemblages remain largely unchanged. This is evident in the dampening of biomass fluctuations at metapopulation and metacommunity scales via a spatial portfolio effect (blue and black trajectories in Fig. S9A), but also in the robustness of species biomass distribution (Fig. S9C) and range size distribution (Fig. S9D, range sizes computed as in Ref. (*16*)). In this case the mean relative biomass and range size are plotted irrespective of species identity (black lines) along with the mean $\pm$ one standard deviation (grey lines), for direct comparison with Ref. (*39*). The relatively small standard deviations demonstrate a temporally robust distribution of metapopulation biomasses and spatial ranges, despite large fluctuations at the local scale.

STAR in large metacommunity models: We characterised the within assemblage STAR using a moving spatio-temporal window as described in the main text and comparing the resulting SAR and STR exponents. In Fig. S10 we show the nested SAR and STR for a single metacommunity of $N = 256$. The number of species detected for large spatial or temporal windows necessarily saturates in closed systems. We therefore defined the exponents of the

573 STAR, displayed in Fig. 4 of the main text, as the maximum slope of the SAR/STR on double
574 logarithmic axes.

Supplementary figures

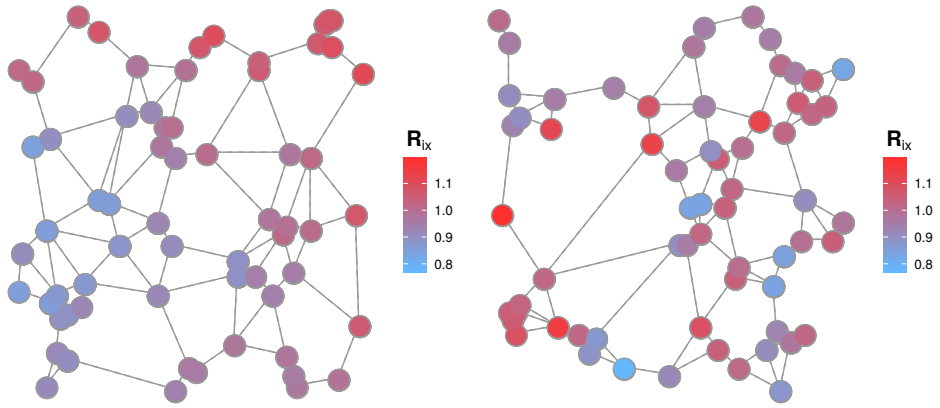

Figure S1: **Spatially autocorrelated growth rate distributions.** Instrinsic growth rates are sampled from spatially autocorrelated random fields of autocorrelation length ϕ and variance σ^2. Two example distributions are shown, both of $N = 64$, $\sigma^2 = 0.01$, with $\phi = 10$ (left) and $\phi = 1$ (right). See Materials and Methods for details.

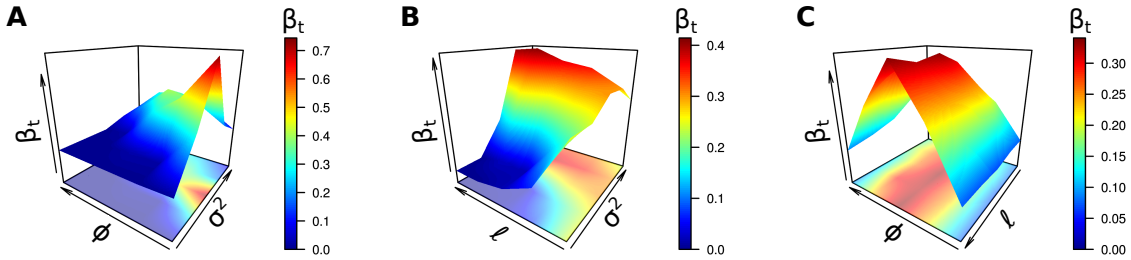

Figure S2: **Temporal turnover throughout the spatial parameter space.** Temporal β-diversity β_t was computed as the mean BC dissimilarity between time points in a time series of 1000 unit times, observed in metacommunities of $N = 64$ patches. Correlation length ϕ was varied in the range 1 to 100, environmental variability σ^2 and dispersal length ℓ in the range 10^{-2} to 1, with each parameter combination replicated 10 times. The values of ϕ, σ^2 and ℓ were each plotted on logarithmic axes. In **A** we fixed ℓ at 0.5; in **B** ϕ at 10; and in **C** σ^2 at 1.0. See Supplementary Text for details.

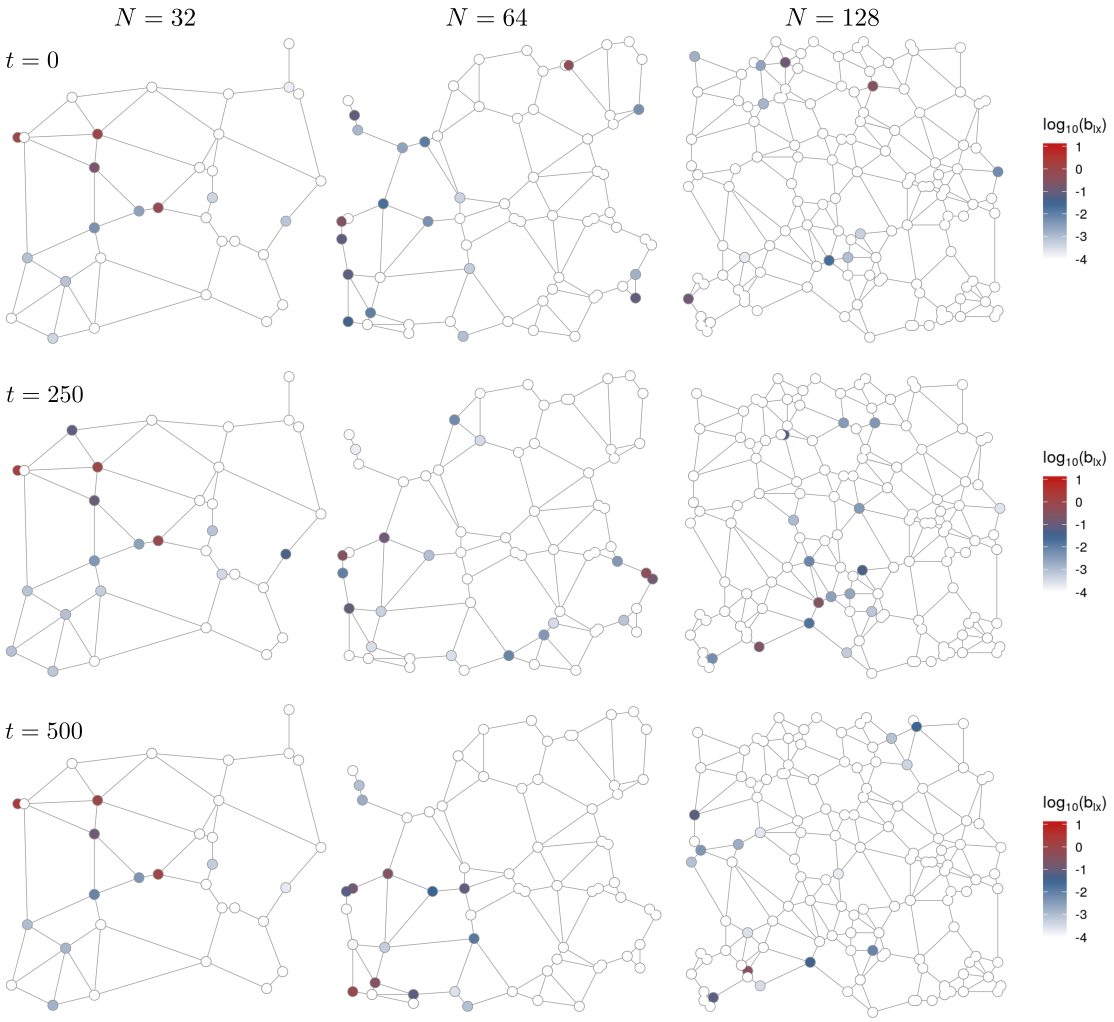

Figure S3: **Autonomous metapopulation dynamics in large metacommunity models.** In species rich metacommunities of $N > 8$ patches, local biomasses autonomously fluctuate and the variability of those fluctuations increases with metacommunity size. Here we show the instantaneous biomass distributions for a single species in metacommunities of $N = 32$, 64 and 128, at three time points in logarithmic biomass units. For $N = 32$, autonomous fluctuations are largely restricted to the outer extremes of the species' distribution, while the core range (left of network) remains largely static. For $N = 64$, some nodes or regions may be permanently occupied by the focal species, however even in this core range biomass can fluctuate by orders of magnitude. With the emergence of Gleasonian turnover in the high N limit no or few nodes are permanently occupied and local community composition is no longer well characterized by the core-transient distinction (*34,36,39*), which decomposes local communities into populations that are present almost all the time, and those observed only rarely. Hence, for $N = 128$ no obvious core range exists. Note that spatial networks are not shown to scale, the area of the model landscape is $\approx N$ in all cases. $A_{ij} = 0.5$ with probability 0.5, $\phi = 10$, $\sigma^2 = 0.01$, $\ell = 0.5$. See Main Text for details.

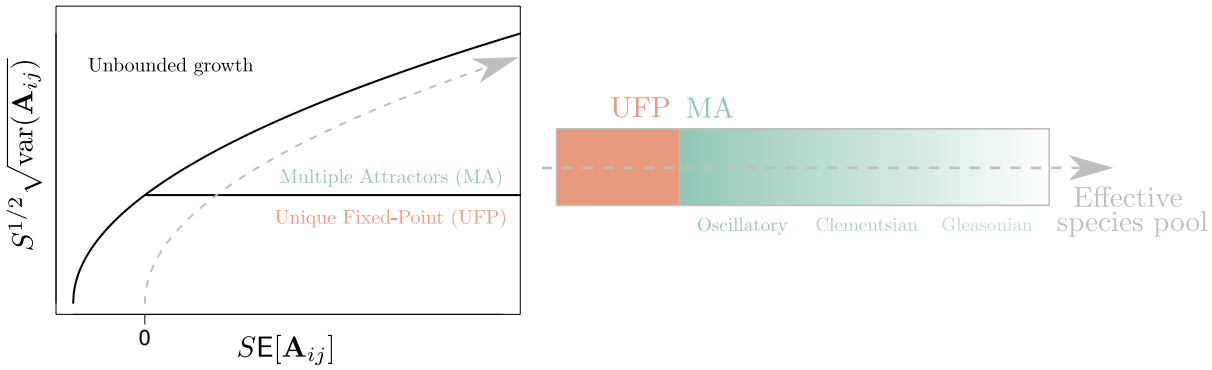

Figure S4: **The sharp transition between UFP and MA phases.** Reproduction of the phase diagram derived by Bunin (*25*) showing the emergence of MA as the size S of the species pool increases. In our case, the first and second moments of the distribution in A_{ij} were fixed. Community state in phase space therefore follows a square root function with increasing S, as indicated by the dashed line. (The "Unbounded growth" phase is hence not relevant for our study.) In spatially explicit metacommunity models we observe the emergence of autonomous turnover which transitions from oscillations to Clementsian and finally Gleasonian turnover. See Supplementary Text for details.

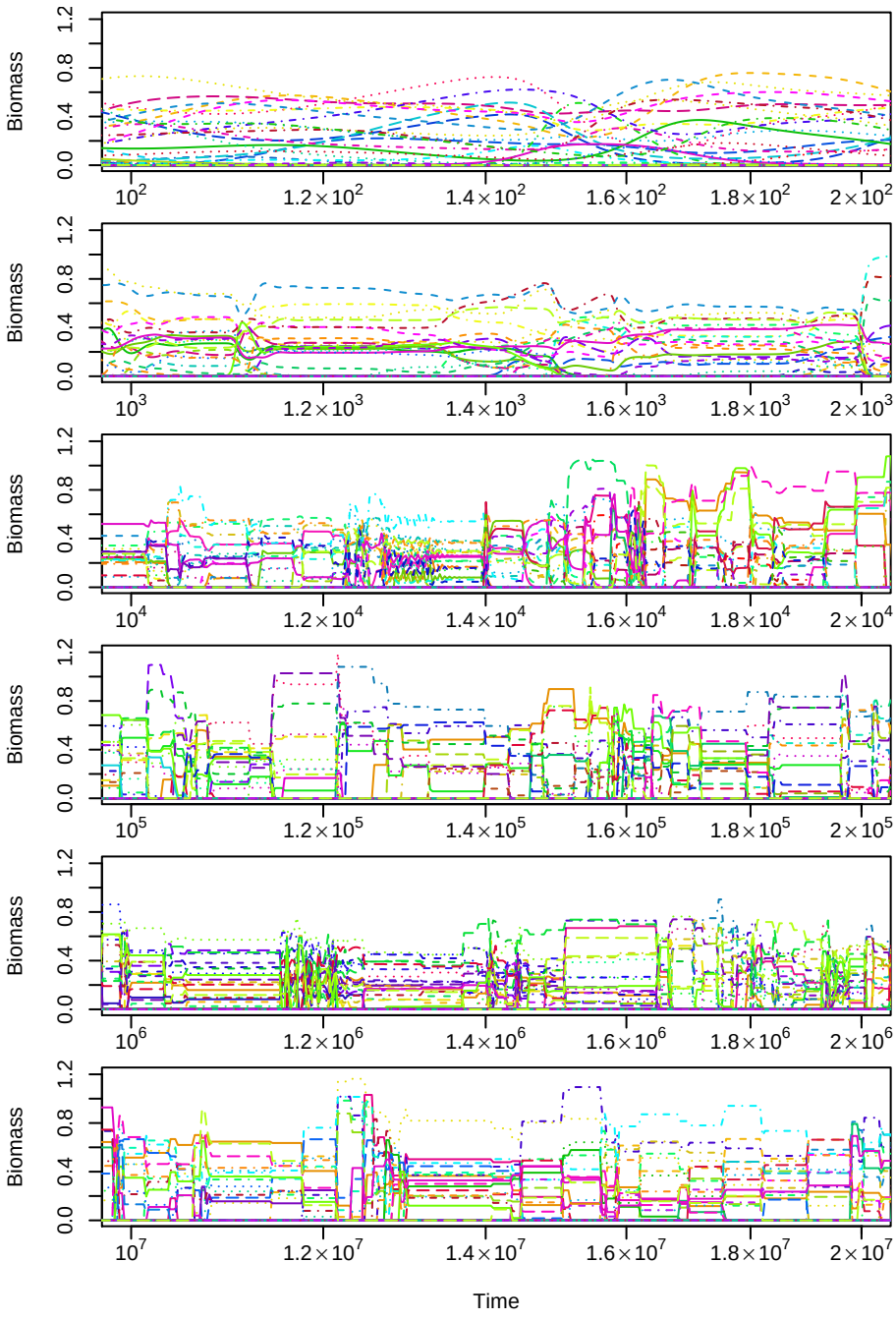

Figure S5: **Episodes in the approach of an isolated LV community model to a heteroclinic network**. The biomasses of different species are represented by lines of different colours and style. At any moment in time, all but a few of the $S = 300$ species in the system have biomasses close to zero. With increasing simulation times t the intervals between the switches in system state, corresponding to transitions from the vicinity of one saddle point to the next, become longer, while the duration of these transitions remains of the order of magnitude of 10 time units, leading to increasingly sharper transitions on the logarithmic time scale. See Supplementary Text for details.

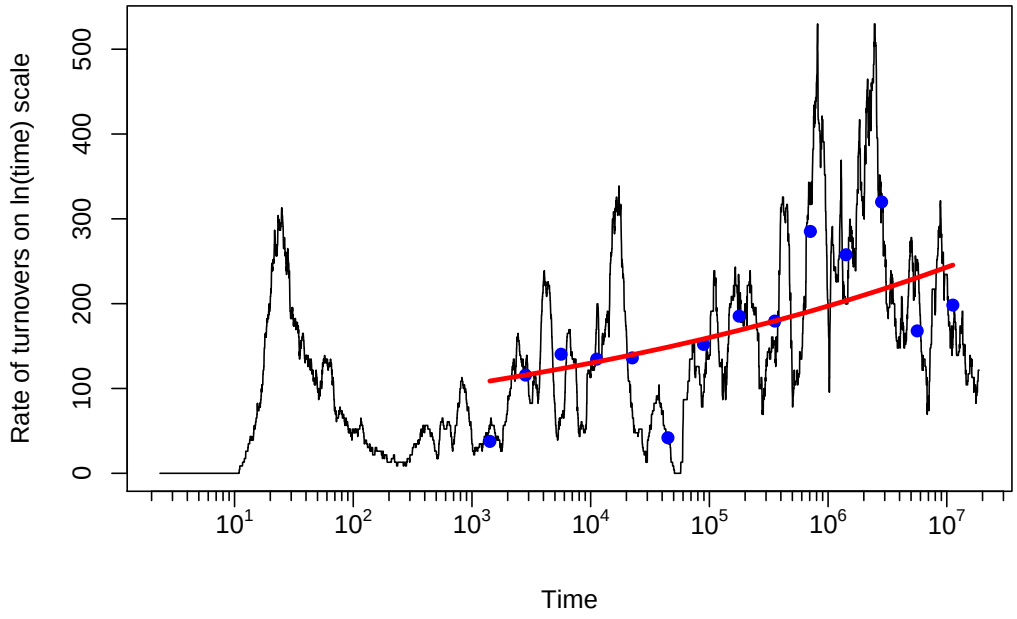

Figure S6: **Rate of change in community composition for the simulation shown in Fig. S5**. The black line is the moving average over 100 subsequent recordings, blue dots represent averages over non-overlapping adjacent blocks of 300 recordings for $t \geq 1000$, and the red line a median nonlinear regression of the dots by a power-law (rate) $\sim t^{\nu}$ ($\nu = 0.091 \pm 0.062$, not significantly different from zero). See Supplementary Text for details.

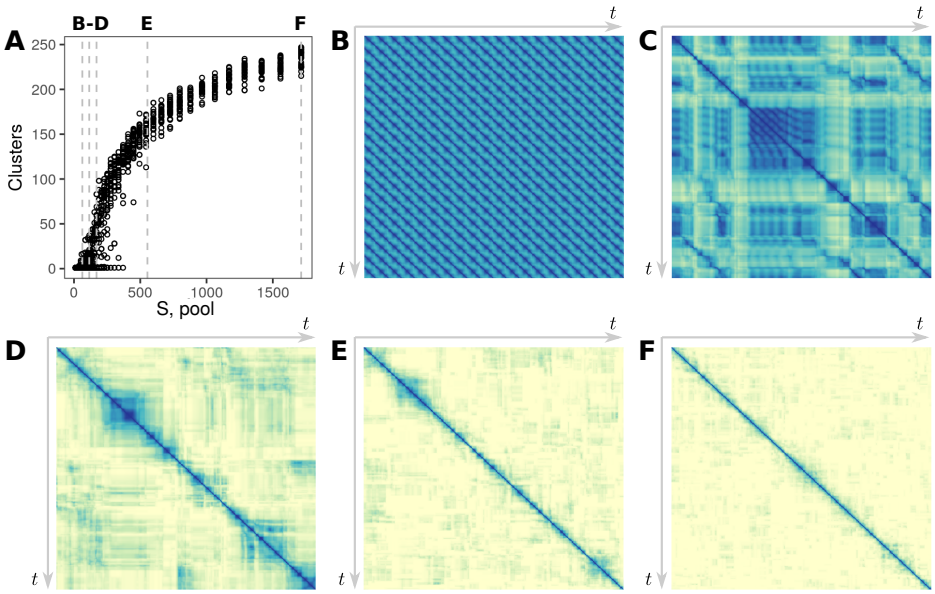

Figure S7: **Autonomous turnover in isolated LV communities**. **A**: The number of compositional clusters detected as a function of the size of the pool of potential invaders for a propagule pressure, ϵ, of 10^{-15} biomass units per unit time. **B**-**F**: Heatmaps of the pairwise Bray-Curtis similarity for the corresponding time-series (over 10^4 unit times) showing a clear transition from oscillatory to Clementsian turnover and finally to Gleasonian turnover. Dashed lines in **A** show the size of the species pool for which each community time series was generated. $A_{ij} = 0.5$ with probability 0.5, $\sigma^2 = 0.01$. The parameters ϕ and ℓ are not defined for the isolated LV models. See Supplementary Text for details.

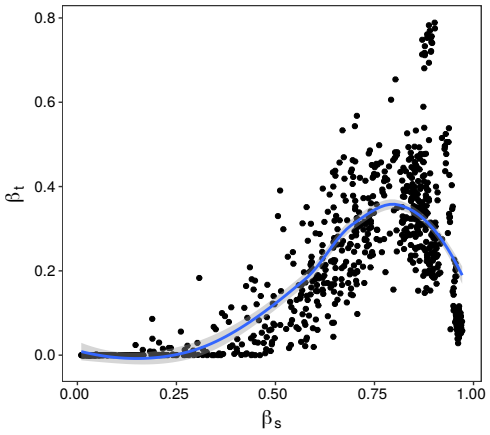

Figure S8: **Unimodal relationship between spatial and temporal turnover.** Spatially averaged temporal turnover plotted against the time averaged spatial turnover in the local neighbourhood, computed during 1000 unit times. Blue line and shaded area represent a locally weighted regression (LOESS smoothing) and 95% C.I.. Parameters N, ϕ, σ^2 and ℓ as in Fig. S2. See Supplementary Text for details.

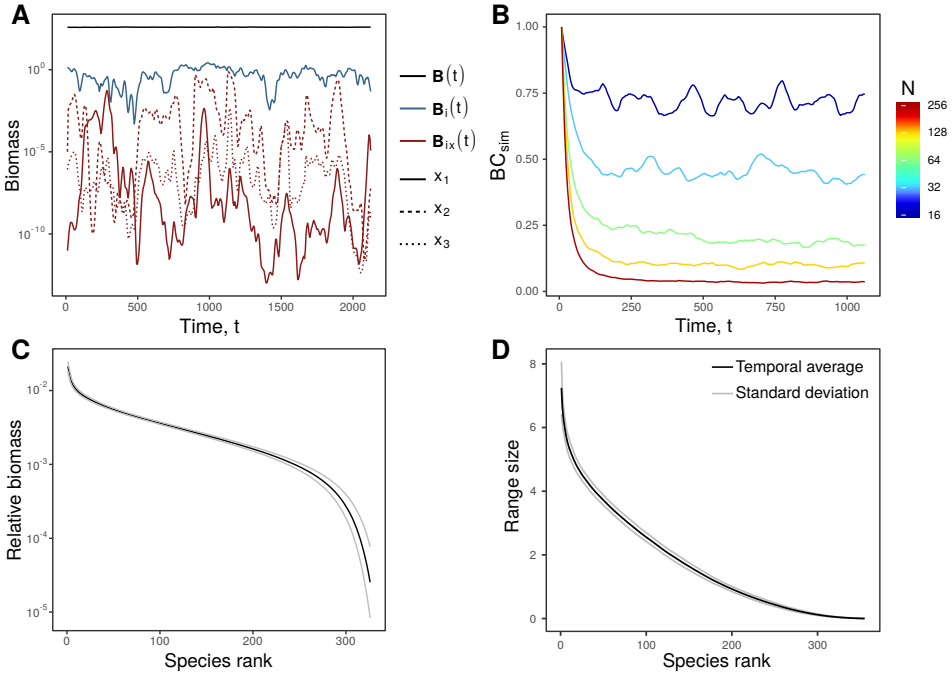

Figure S9: **Temporally robust community structure A**: We highlight the scale dependence of autonomous population dynamics by showing the biomass of three random local populations of the same species (B_{ix}, red), of the metapopulation of which they form a part ($\mathrm{B}_i = \sum_x \mathbf{B}_{ix}$, blue) and finally of the entire metacommunity ($\mathrm{B} = \sum_i \sum_x \mathbf{B}_{ix}$), black). **B**: Autonomous turnover can be substantial. Here we show the decay of spatially averaged BC similarity from an arbitrary initial composition in metacommunities of $N = 16$, 32, 64, 128, and 256 patches. For large metacommunities undergoing autonomous Gleasonian turnover, the percentage of permanent populations, and hence the temporal BC similarity can drop to zero. **C**: Metacommunity scale relative rank abundance curve, plotted with species 'identity' disregarded. The black curve represents the mean biomass observed at a given rank, while grey curves represent the mean $\pm$ one standard deviation. This figure highlights the temporally invariant diversity structure at the metacommunity scale. **D**: The temporally averaged rank range size curve, plotted as in C. $A_{ij} = 0.5$ with probability 0.5, $\phi = 10$, $\sigma^2 = 0.01$, $\ell = 0.5$. $N = 64$ for **A**, **C** and **D**. See Supplementary Text for details.

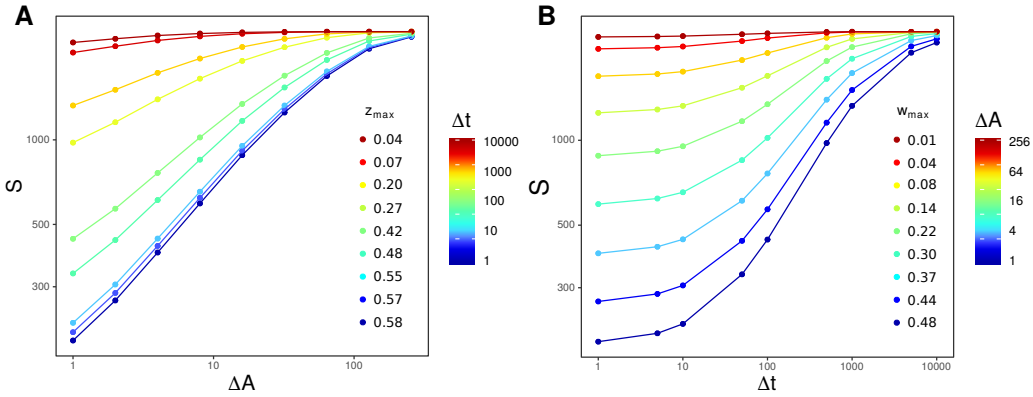

Figure S10: **The Species-Time-Area-Relation.** The nested SAR (**A**) and STR (**B**) generated using a sliding window approach for a single metacommunity model of $N = 256$. Metacommunity models are closed systems and as such, both the SAR and STR saturate for the large sub-samples. As such we defined the exponents of the STAR by the maximum slopes observed on double logarithmic axes. $A_{ij} = 0.5$ with probability 0.5, $\phi = 10$, $\sigma^2 = 0.01$, $\ell = 0.5$. See Supplementary Text for details.